Biomedical Optics EXPRESS

Multispectral nanoparticle contrast agents for true-color spectroscopic optical coherence tomography

You Leo Li,[1] Kevin Seekell,[1] Hsiangkuo Yuan,[1] Francisco E. Robles,[2] and Adam Wax[1,*]

[1]*Department of Biomedical Engineering and Fitzpatrick Institute for Photonics, Duke University, Durham NC 27708, USA*
[2]*Department of Chemistry, Duke University, Durham NC 27708, USA*
*a.wax@duke.edu

Abstract: We have recently developed a novel dual window scheme for processing spectroscopic OCT images to provide spatially resolved true color imaging of chromophores in scattering samples. Here we apply this method to measure the extinction spectra of plasmonic nanoparticles at various concentrations for potential *in vivo* applications. We experimentally demonstrate sub-nanomolar sensitivity in the measurement of nanoparticle concentrations, and show that colorimetric imaging with multiple species of nanoparticles produces enhanced contrast for spectroscopic OCT in both tissue phantom and cell studies.

OCIS codes: (110.4500) Optical coherence tomography; (160.4236) Nanomaterials; (300.1030) Absorption.

References and Links

1. M. Hu, J. Chen, Z.-Y. Li, L. Au, G. V. Hartland, X. Li, M. Marquez, and Y. Xia, "Gold nanostructures: engineering their plasmonic properties for biomedical applications," Chem. Soc. Rev. **35**(11), 1084–1094 (2006).
2. A. L. Oldenburg, M. N. Hansen, D. A. Zweifel, A. Wei, and S. A. Boppart, "Plasmon-resonant gold nanorods as low backscattering albedo contrast agents for optical coherence tomography," Opt. Express **14**(15), 6724–6738 (2006).
3. A. L. Oldenburg, M. N. Hansen, T. S. Ralston, A. Wei, and S. A. Boppart, "Imaging gold nanorods in excised human breast carcinoma by spectroscopic optical coherence tomography," J. Mater. Chem. **19**(35), 6407–6411 (2009).
4. F. E. Robles, S. Chowdhury, and A. Wax, "Assessing hemoglobin concentration using spectroscopic optical coherence tomography for feasibility of tissue diagnostics," Biomed. Opt. Express **1**(1), 310–317 (2010).
5. F. E. Robles, C. Wilson, G. Grant, and A. Wax, "Molecular imaging true-colour spectroscopic optical coherence tomography," Nat. Photonics **5**(12), 744–747 (2011).
6. R. N. Graf, W. J. Brown, and A. Wax, "Parallel frequency-domain optical coherence tomography scatter-mode imaging of the hamster cheek pouch using a thermal light source," Opt. Lett. **33**(12), 1285–1287 (2008).
7. A. Wax, C. Yang, R. R. Dasari, and M. S. Feld, "Measurement of angular distributions by use of low-coherence interferometry for light-scattering spectroscopy," Opt. Lett. **26**(6), 322–324 (2001).
8. F. Robles, R. N. Graf, and A. Wax, "Dual window method for processing spectroscopic optical coherence tomography signals with simultaneously high spectral and temporal resolution," Opt. Express **17**(8), 6799–6812 (2009).
9. B. Duncan, C. Kim, and V. M. Rotello, "Gold nanoparticle platforms as drug and biomacromolecule delivery systems," J. Control. Release **148**(1), 122–127 (2010).
10. A. K. Salem, P. C. Searson, and K. W. Leong, "Multifunctional nanorods for gene delivery," Nat. Mater. **2**(10), 668–671 (2003).
11. A. P. Leonov, J. Zheng, J. D. Clogston, S. T. Stern, A. K. Patri, and A. Wei, "Detoxification of gold nanorods by treatment with polystyrenesulfonate," ACS Nano **2**(12), 2481–2488 (2008).
12. K. Seekell, H. Price, S. Marinakos, and A. Wax, "Optimization of immunolabeled plasmonic nanoparticles for cell surface receptor analysis," Methods **56**(2), 310–316 (2012).
13. A. Curatolo, B. F. Kennedy, and D. D. Sampson, "Structured three-dimensional optical phantom for optical coherence tomography," Opt. Express **19**(20), 19480–19485 (2011).
14. M. C. Skala, M. J. Crow, A. Wax, and J. A. Izatt, "Photothermal optical coherence tomography of epidermal growth factor receptor in live cells using immunotargeted gold nanospheres," Nano Lett. **8**(10), 3461–3467 (2008).

#170037 - $15.00 USD Received 7 Jun 2012; revised 18 Jul 2012; accepted 18 Jul 2012; published 20 Jul 2012

15. H. Yuan, A. M. Fales, and T. Vo-Dinh, "TAT peptide-functionalized gold nanostars: enhanced intracellular delivery and efficient NIR photothermal therapy using ultralow irradiance," J. Am. Chem. Soc. **134**(28), 11358–11361 (2012).
16. A. C. Curry, M. Crow, and A. Wax, "Molecular imaging of epidermal growth factor receptor in live cells with refractive index sensitivity using dark-field microspectroscopy and immunotargeted nanoparticles," J. Biomed. Opt. **13**(1), 014022 (2008).
17. K. Seekell, M. J. Crow, S. Marinakos, J. Ostrander, A. Chilkoti, and A. Wax, "Hyperspectral molecular imaging of multiple receptors using immunolabeled plasmonic nanoparticles," J. Biomed. Opt. **16**(11), 116003 (2011).

1. Introduction

Spectroscopic optical coherence tomography (SOCT) is a technique that combines the high-resolution, noninvasive, three-dimensional imaging capability of optical coherence tomography (OCT) with the ability to obtain spectral information about a sample. In order to enhance the diagnostic ability of SOCT, there has been great interest in the development of contrast agents that can be used to label biological tissues to increase optical contrast compared with traditional OCT methods. Recently, gold nanorods and nanocages have been demonstrated to enhance optical contrast for SOCT in tissue phantoms [1,2] and *ex vivo* tissues [3]. Compared to small fluorescent molecules, such as sodium fluorescein, nanoparticles have drug loading capability and the potential for active cellular targeting, which make them ideal for tumor cell imaging and drug delivery. However, these previous efforts in using nanoparticles as contrast agents for SOCT have utilized infrared light sources, and thus have not exploited the ability to obtain simultaneous contrast from endogenous absorbers such as hemoglobin, which absorbs primarily in the visible region of the spectrum and is a compelling target for biomedical applications [4,5]. An alternative to these techniques is molecular imaging true-color spectroscopic (METRiCS) OCT which uses a wide spectral bandwidth laser source centered in the visible spectrum and the dual window (DW) processing method [5], which reveals spatially resolved spectroscopic information with high resolution in both the spatial domain and the spectral domain. This approach has been demonstrated to provide contrast from endogenous absorbers, such as oxygenated and deoxygenated hemoglobin [4], as well as exogenous absorbers *in vivo* [5]. In addition, the wide bandwidth in METRiCS OCT enables high depth resolution, greater than that seen with most OCT systems operating in the infrared region of the spectrum. Here we report on the measurements of extinction coefficients and quantification of gold nanosphere and gold nanorod concentrations using the DW processing method, the basis of METRiCs OCT. Moreover, we demonstrate the enhanced true color contrast provided by this method in combination with nanoparticles of varying types in tissue phantoms and cells.

2. Instrumentation and materials

Our device setup is based on a parallel Fourier-domain OCT (pfdOCT) system, which uses an imaging spectrograph that allows simultaneous detection of multiple spectrograms in parallel [6]. In this particular system, a super-continuum laser source (Fianium, SC450) is used, where light from the laser source is filtered to produce a center wavelength of 575 nm and a bandwidth of 240 nm. The filtered light is input to the pfdOCT system, which is based on a Michelson interferometer with the addition of a 4-f imaging system (Fig. 1) [7]. Here, light from the source is collimated by lens, L1, and then focused on one axis by a cylindrical lens, L2. L3 and L4 are used to form a line of illumination on the sample and reference arm, respectively. The scattered light returned from the sample is combined with the reflected light from the reference arm at the beam-splitter and imaged onto the entrance slit of the spectrograph. With this setup, up to 400 interferograms, limited by the CCD and beam size, are sampled in parallel. An axial resolution of 1.2 μm and a transverse resolution of 6.9 μm were determined experimentally.

Data collected by the CCD are processed with the DW method, which is a bilinear processing approach that produces spatially resolved spectroscopic information with high

#170037 - $15.00 USD Received 7 Jun 2012; revised 18 Jul 2012; accepted 18 Jul 2012; published 20 Jul 2012

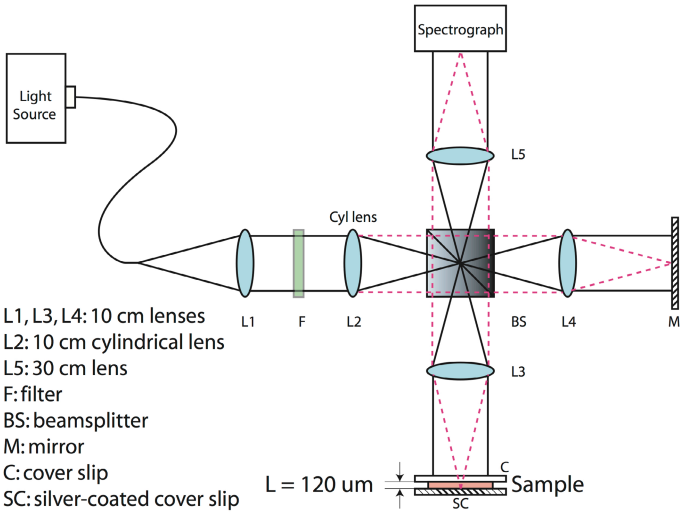

Fig. 1. Parallel frequency domain OCT system and sample. L = 120 μm is the thickness of the sample used in the concentration measurement. Red dashed lines and black lines show the propagation of light in two orthogonal dimensions.

resolution in both the spatial and spectral domains [8]. In this method, two short-time Fourier transforms (STFTs) are computed, one using a wide spectral window (Δk_w = 0.907 μm) and another using a narrow spectral window (Δk_w = 0.016 μm). The two resulting time-frequency distributions (TFDs) are then multiplied on a point-by-point basis, forming a TFD with high resolutions in both domains. Thus, the DW method avoids the trade-off between spatial and spectral resolutions that is associated with the use of a single STFT and approaches the high resolution seen for Cohen's bilinear distributions (e.g., the Wigner distribution) as representations of time frequency distributions. We have shown that this method is equivalent to probing the Wigner distribution of the scattered sample field with two orthogonal windows that independently adjust the spatial and spectral resolutions [8]. METRiCs OCT, which utilizes the DW method, has been applied to produce true-color, quantitative, tomographic images of an *in vivo* rat dorsal skin fold window chamber model [5]. Quantification of hemoglobin oxygen saturation levels of the vasculature was also demonstrated [4].

The nanoparticles used in this study are gold nanospheres (GNS, BBInternational, 60 ± 3 nm) and gold nanorods (GNR). These nanoparticles have been extensively studied in drug delivery [9] or gene delivery [10], and do not exhibit cytotoxicity with proper polymer coating [11]. The GNS has an extinction peak at 535 nm in deionized water. The synthesis of nanorods follows the standard seed-mediated method [12]. Two batches of GNR were used. The aspect ratio of the first batch of rods is manually measured from TEM images of 110 nanorods to be 1.55 ± 0.26, with the longitudinal axes having the size of 55.5 ± 10.2 nm, and the transverse axes 36.2 ± 7.2 nm; the aspect ratio of the second batch is 1.48 ± 0.27, with the longitudinal axes being 57.6 ± 11.4 nm and the transverse axes being 39.6 ± 8.2 nm. Both batches of GNR have an extinction peak at 603 nm in deionized water.

3. Experimental methods and results

3.1. Concentration measurement

To demonstrate the limits of detection of these nanoparticles using METRiCS OCT, various concentrations of the nanoparticles are prepared in a solvent of deionized water (DI)/glycerol (vol/vol = 1:9, and refractive index n = 1.461). Glycerol is use here to increase the viscosity of solvent and hence minimize the potential of fringe washout effects induced by the Brownian motion of the nanoparticles.

#170037 - $15.00 USD Received 7 Jun 2012; revised 18 Jul 2012; accepted 18 Jul 2012; published 20 Jul 2012

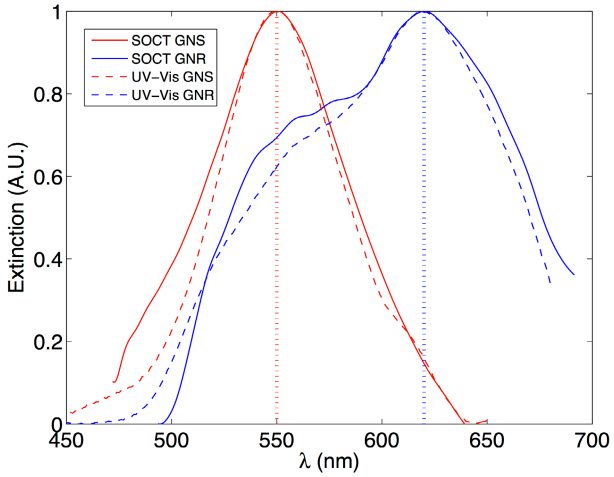

Fig. 2. Extinction spectra (μ) of the nanospheres and nanorods in DI/glycerol. The solid curve represents the curves obtained with METRiCS OCT (labeled as SOCT) technique, and the dashed curved is obtained from Cary 300 Bio UV-Vis Spectrometer (Agilent Technologies, Santa Clara, US). The GNS shows an extinction peak at 550 nm and the GNR shows an extinction peak at 620 nm in DI/glycerol, both red-shifted compared to the peaks seen in pure DI water. All the curves were normalized for better illustration. Note that the NPs are mostly absorbing, so GNS should appear red and GNR should appear blue when observed in a transmission mode measurement. The discrepancy in the width of the spectra is caused by (1) the lower SNR in the short wavelength and long wavelength portions of the spectra, and (2) the normalization of the signal.

For the measurement of nanoparticle extinction, we use a sample container composed of one coverslip (top) and one silver-coated coverslip (bottom), separated with a spacer of thickness L = 120 μm, which is also the thickness of the nanoparticle colloid. Data are collected with our pfdOCT system and then processed with the DW method.

The concentrations of the nanoparticles are calculated by first computing the extinction coefficients $\mu(\lambda)$, from the Beer-Lambert law:

$$\mu(\lambda) = -\frac{1}{L} \cdot \ln\left(\frac{I(\lambda)}{I_0(\lambda)}\right) \tag{1}$$

where $I_0(\lambda)$ and $I(\lambda)$ are the reflected spectra from a sample containing solvent only (control sample) and the spectra from the sample containing nanoparticles, respectively. For each of the samples, we analyzed the absorption profiles of 128 distinct spatial locations obtained from two separate acquisitions (i.e. B-scans), each with a 20 ms exposure. Then an average absorption spectrum was computed. The extinction coefficients are expressed in terms of the concentration and the molar extinction coefficients of the nanoparticles:

$$\mu = C \cdot \varepsilon(\lambda) / \log_{10}(e) \tag{2}$$

in which C is the concentration of the nanoparticles and $\varepsilon(\lambda)$ is the extinction spectrum of the particles.

Note that the molar extinction coefficients, ε, are independent of the path length and concentration. Figure 2 shows the extinction spectra obtained with our method along with the spectra measured with a UV-Vis spectrometer. As the figure shows, the spectra obtained with both methods are in excellent agreement, where the GNS and GNR in DI/glycerol exhibit resonance peaks at 550 nm and 620 nm, respectively. The NPs are mostly absorbing, so GNS should appear red and GNR should appear blue when observed in a transmission mode measurement.

#170037 - $15.00 USD Received 7 Jun 2012; revised 18 Jul 2012; accepted 18 Jul 2012; published 20 Jul 2012

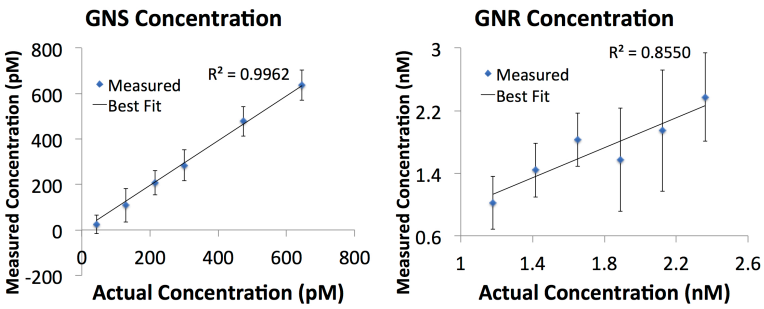

Fig. 3. Measured concentrations of the gold nanospheres (GNS) and the gold nanorods (GNR). The error bars reflect the standard deviations obtained from 128 measurements.

The nanoparticle concentrations in the phantoms are calculated by taking the extinction spectrum as a function of wavelength and fitting data to a line of the form $y = m \cdot x$, using a linear least squares method, as previously done in Ref. [4]. In this equation, x are the extinction spectra of the particles and m is related to nanoparticle concentration, C, through $m = C \cdot L$, in which L is the thickness and can be measured from imaging. This procedure is carried out for both samples and the results are summarized in Fig. 3. We find that the measured and expected concentrations are in good agreement, with the slopes for the lines being close to 1 (0.98 for GNS and 0.96 for GNR), indicating that the measured concentration matches the expected values. The correlation coefficient for the line of best fit is $R^2 = 0.9962$ for GNS and $R^2 = 0.8550$ for GNR, both showing a strong correlation.

The limits of detection (LODs) are represented by the average standard deviations, which are 60.9 pM for GNS and 0.5 nM for GNR.

3.2. Tissue phantom experiments

To demonstrate the feasibility of using GNS and GNR as colorimetric contrast agents, tissue phantoms are imaged using our system. While the previous section shows that our device can measure NP concentration, this section shows that NPs can be used as colorimetric contrast agents in tissue phantoms with relatively high scattering cross-section. As is shown in Fig. 4(a), the phantom consists of three layers of structures: The top layer consists of Intralipid (2%) and Agar (2%); the middle layer is Agar (2%) with GNS (2.3 nM) or GNR (6.3 nM); and the bottom layer is made up of TiO_2 (1%) and Agar (2%), which has a larger scattering coefficient of 14.3 mm^{-1}, to simulate the scattering of human tissue [13], and ensures that light returns from these deeper sample depths. Data are acquired from the phantoms using the pfdOCT system and processed with the method described in [8] to produce true-color images. Specifically, the spectrum of each spatial point is extracted from the interferograms with the DW method, and then divided into red, blue and green channels using the Commission Internationale d'Eclairage (CIE) color functions. Then the color information is superposed with the OCT image to produce a true-color OCT image.

The resulting true-color OCT images are shown in Fig. 4(d) and (e). The results indicate that nanoparticles provide color contrast even when no significant intensity contrast can be observed. The blue color is produced by GNR, and the red is produced by GNS. Therefore, different regions are differentiable with a simple visual inspection. In addition, the color of the scattered light from the phantom within and beneath the layer with nanoparticles agrees with the results of spectral measurements in Fig. 2.

Next, we quantify the spatially resolved spectroscopic information. In order to do this, the spectra corresponding to two slices at the same depth of the sample are used. One spectrum (noted as I_{NP}) is from the region doped with nanoparticles and the other spectrum (noted as $I_{control}$) is from the region without nanoparticles. The spectra can be represented as

#170037 - $15.00 USD Received 7 Jun 2012; revised 18 Jul 2012; accepted 18 Jul 2012; published 20 Jul 2012

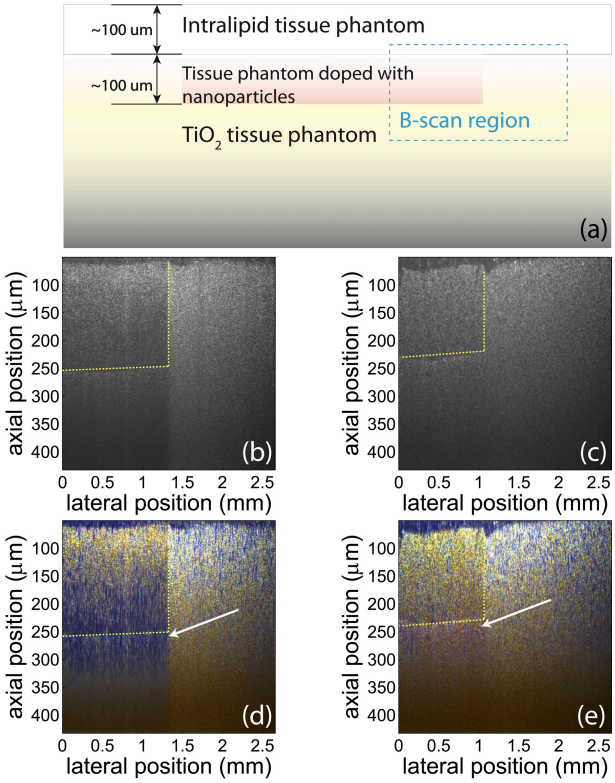

Fig. 4. (a): Schematic of sample structure. The tissue phantom has three layers: Intralipid/agar layer on top, NP/agar layer in the middle, and TiO_2 /agar layer in the bottom. The B-scan is taken in the region in the blue rectangle. (b) and (c): Conventional OCT images of the tissue phantoms with GNR (b) and GNS (c). The regions with different species of nanoparticles are not differentiable in conventional OCT images. Yellow lines indicate the approximate position of the interfaces between regions with and without NPs. (d) and (e) True-color OCT images of the same region as shown in (b) and (c), respectively. The color contrast produced with the nanoparticles can help differentiate the regions with different NPs and the region without any NPs. The blue color (white arrow) is produced by GNR, and the red color (white arrow) is produced by GNS. Note that the concentration of GNR (6.3 nM) is higher than the concentration of GNS (2.3 nM). Also, the absorption of GNR is stronger than GNS. Therefore, color contrast starts to be visible at a lower depth in (d) than in (e).

$$I_{NP}(\lambda) = I_0(\lambda)\cdot\exp(-(\mu_{NP}(\lambda)+\mu_{phantom}(\lambda))\cdot L)\cdot S(\lambda)$$
$$I_{control}(\lambda) = I_0(\lambda)\cdot\exp(-\mu_{phantom}(\lambda)\cdot L)\cdot S(\lambda) \quad (3)$$

in which I_0 is the source spectrum; μ_{NP} and $\mu_{phantom}$ are the extinction coefficient of the nanoparticles and the phantom (without nanoparticles), respectively; and $S(\lambda)$ is the wavelength dependent backscattering term. Note that because the backscattering term varies more slowly than the attenuation term, $S(\lambda)$ may be assumed to be approximately equal for the NPs and the phantom. Still, a more accurate result is obtained if the spectra are obtained from depths corresponding to regions below the nanoparticle layer, where the backscattering due to the phantom accurately accounts for the scattering by agar and TiO_2. Thus, the extinction coefficient of the nanoparticles may be expressed as

$$\mu_{NP}(\lambda) = -\frac{1}{L}\cdot\log\left(\frac{I_{NP}(\lambda)}{I_{control}(\lambda)}\right) \quad (4)$$

#170037 - $15.00 USD Received 7 Jun 2012; revised 18 Jul 2012; accepted 18 Jul 2012; published 20 Jul 2012

To demonstration the fidelity of the spectral information, data from slices more than 200 μm deep in the GNS and the GNR samples are presented. A typical slice has the dimension of 55 μm (axial) × 2.6 mm (lateral). The averaged backscattering spectra from several slices ($I_{Control}(\lambda)$, $I_{NP}(\lambda)$, and $\mu_{NP}(\lambda)$) are shown in Fig. 5. As shown, the extinction spectra (green curves) obtained with our method are in good agreement with those shown in Fig. 2.

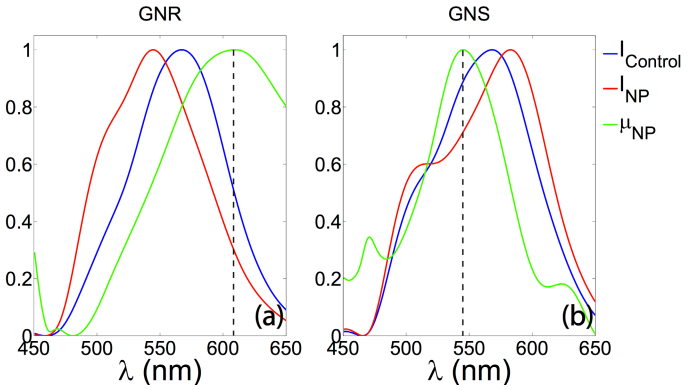

Fig. 5. Spatially resolved spectroscopic information extracted from the tissue phantom containing different species of NPs. Left: spectra from the sample containing GNR. The peak of the extinction curve (green) has a peak at 609 nm, which is shifted 6 nm from its extinction peak in DI water. Right: spectra from the sample containing GNS. The extinction peak at 545.5 nm which is shifted 10.5 nm shift from its extinction peak in DI water. All the curves are normalized for better illustration.

3.3. Cell experiments

Cell experiments have also been conducted as a proof of concept for using nanoparticles as colorimetric contrast agents within cells using the METRiCS OCT system. In order to deliver the nanoparticles into cells, the nanoparticles are first coated with polymers and then functionalized with cell penetrating peptides. After that, the nanoparticles are delivered to cells which are then integrated into three-dimensional constructs [14] and imaged with the METRiCS OCT system.

For the coating of the particles, thiol-terminated polyethylene glycol (SH-PEG, MW 5000, Sigma Aldrich) is added to the colloid of GNS, and then kept at room temperature for 2 hours prior to centrifuge washing to remove excessive PEG from the solution. Polystyrene sulfonate (PSS, MW 70,000, Sigma Aldrich) is added to GNR colloid and kept for 24 hours prior to centrifuge to remove excess. The zeta-potential of PSS coated GNRs is measured to be −43 mV, indicating high stability. After characterization, cysteine-terminated trans-activating transcriptional activator (cysteine-TAT), a type of cell penetrating peptide, is added to the colloid, and then kept for 24 hours prior to centrifuge wash, in order to functionalize the particles to facilitate cellular uptake [15].

The coated and functionalized particles are added to the flasks containing 85% confluent BT549 cells. The particle concentrations are 2 nM for GNS and 0.32 nM for GNR. These concentrations have been carefully chosen so as to produce strong color contrast while keeping the cells alive. After 24 hours of incubation, the cells are washed with phosphate buffered saline (PBS) to remove excessive particles in the medium and then trypsinized and centrifuged. A typical measured survival rate of these cells is 89%. Hyperspectral darkfield images [12] and phase contrast images (Fig. 6) of the cells incubated with NPs, taken prior to trypsinization, show the co-localization of the cells and particles, indicating the cellular uptake of the particles. Note that dark field microscopy detects scattered light, so the color of NPs in these image are different from those in images obtained with METRiCS OCT, which show the absorption of the NPs.

#170037 - $15.00 USD Received 7 Jun 2012; revised 18 Jul 2012; accepted 18 Jul 2012; published 20 Jul 2012

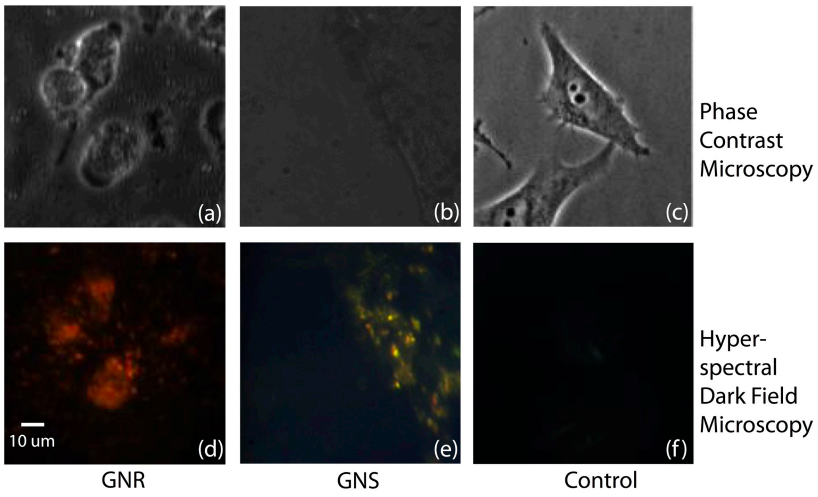

Fig. 6. Phase contrast images (top) and hyperspectral darkfield images (bottom) of cells incubated with NPs. Left: images of cells incubated with GNR. Middle: images from cells incubated with GNS. The bright spots in (d) and (e) indicate the positions of the nanoparticles and the color indicates the peak of their scattering spectra. Right: images from the cells without GNR or GNS. Note that dark field microscopy detects scattered light, so the color of NPs in these image are different from those in images obtained with METRiCS OCT, which show the absorption of the NPs.

The cells are spun down in a centrifuge to yield a numerical density of 10^8 cells/mL and then mixed with low gelling point agar according to an established method [14]. As shown in Fig. 7, the cells are then made into three-dimensional cell constructs. The cells with GNS are shaped to be a layer of 100 μm thick, embedded into the TiO_2 phantom and then imaged. The cells with GNR are made into a construct thicker than the axial field of view of our system, and then imaged. In addition, a control sample made with cells without nanoparticles is also imaged.

As shown in Fig. 7, the nanoparticles provide additional contrast for identifying cellular regions. In addition, as shown in Fig. 8, extinction spectra can also be extracted from more than 200 μm deep in the GNS and GNR sample in the same manner as described in the tissue experiment section, providing additional specificity. As shown in Fig. 8(a) and (b), the extinction peaks for GNR and GNS within the cells are 606 nm and 537 nm, respectively. As shown in Fig. 8(c), spectra from the sample containing cells without any NPs exhibit decreasing scattering with wavelength, the typical extinction trend seen for cell features.

#170037 - $15.00 USD Received 7 Jun 2012; revised 18 Jul 2012; accepted 18 Jul 2012; published 20 Jul 2012

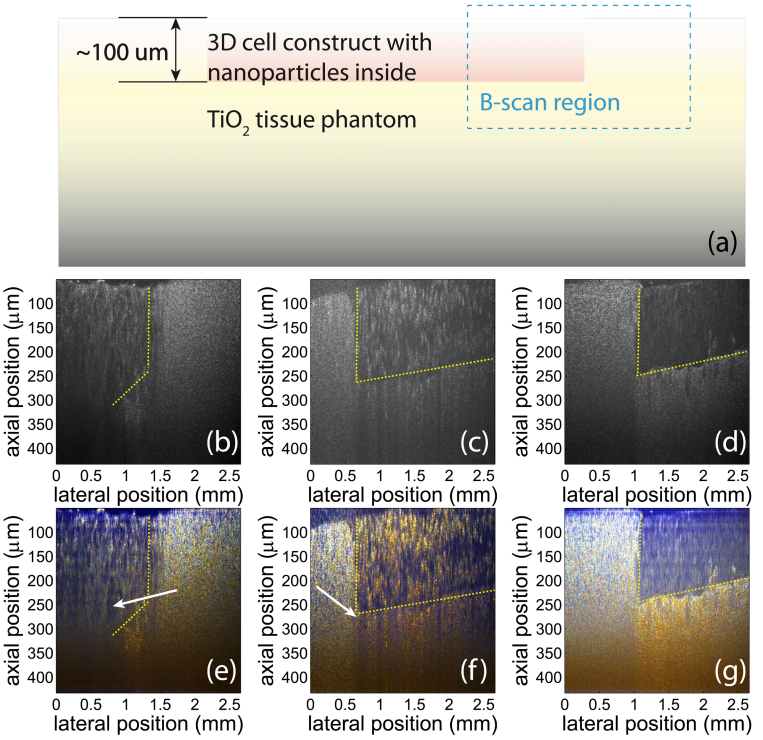

Fig. 7. (a): Schematic of the three-dimensional cell construct. The cell construct has two parts: cell/agar construct, and TiO_2 /agar as control. The B-scan is taken in the interface region indicated by the blue rectangle. (b), (c) and (d): Conventional OCT images of the B-scan. The images are taken from phantoms with GNR (b), GNS (c), and no NPs (d). (e), (f), and (g): True color OCT images of the corresponding B-scans. The color contrast produced with the nanoparticles can help differentiate the regions with cells filled with different species of NPs, as wells as from the cells without any NPs. The blue color is produced by GNR, and the red is produced by GNS.

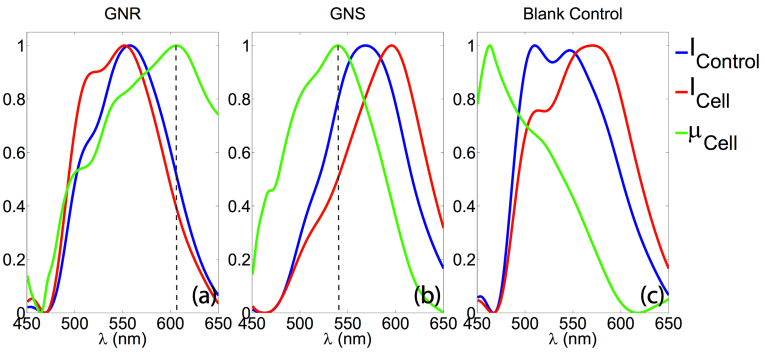

Fig. 8. Spatially resolved spectroscopic information extracted from the tissue phantoms containing different species of NPs. (a): spectra from the sample containing cells incubated with GNR. The peak of the extinction curve (green) is at 606 nm, showing a 3 nm shift from its extinction peak in DI water. (b): spectra from the sample containing cells with GNS. The extinction peak (green) is at 537.1 nm, which has a 2.1 nm shift from its extinction peak in DI water. (c): spectra from the sample containing cells without any NPs, exhibiting decreasing scattering with wavelength, the typical extinction trend seen for cell features. All curves are normalized.

#170037 - $15.00 USD Received 7 Jun 2012; revised 18 Jul 2012; accepted 18 Jul 2012; published 20 Jul 2012

4. Discussion

As shown, METRiCS OCT system has the capability to extract the extinction spectra of multiple species of gold nanoparticles to produce colorimetric and spectral contrast in three dimensions. The analysis presented here shows that it can discriminate concentrations of nanoparticles down to the sub-nanomolar level. In addition, the high resolution and intuitive true color display of our system makes it a potentially useful functional imaging modality for detecting nanoparticle contrast agents.

The higher standard deviation and lower R^2 associated with GNR as compared to the GNS, as shown in Fig. 3, might be ascribed to their wide distribution of aspect ratios. In addition, our LODs are estimated to be 80.0 ppm for GNR and 259.8 ppm for GNR. As a comparison, Skala et al. reported an LOD of 14 ppm of GNS with a photothermal OCT system [14] and Oldenburg et al. reported an LOD of 30 ppm of GNR with their OCT setup [2]. However, given the significantly longer acquisition times used in those experiments, an operation equivalent to more averaging, we expect to see higher LODs for our experiments. In experiments with comparable acquisition times, we expect that our approach would produce lower LODs than these previous efforts.

The extinction peaks of the GNR and GNS in the tissue phantom and cell experiments, as shown in Fig. 5 and Fig. 8, respectively, are red shifted from the corresponding peak locations with DI water as the solvent. This red shift is expected due to changes in the dielectric environment of the NPs [16]. In addition, the yellow color seen below the cell layer in Fig. 7(g), as well as the extinction spectra of cells without NPs shown in Fig. 8, agrees with the general optical extinction properties of cells.

5. Conclusion

We applied METRiCS OCT to measure the extinction spectra of plasmonic nanoparticles at various concentrations for potential *in vivo* applications. As previously mentioned, nanoparticles are of great interest to the biomedical community. Their drug loading capability, potential for active cellular targeting, and high biocompatibility make them an ideal multifunctional platform for simultaneous molecular contrast imaging and drug delivery. As demonstrated in this work, METRiCS OCT provides a unique method to identify different types of nanoparticles based on their optical absorption properties potentially for tumor cell imaging, monitoring treatment therapies (e.g. using photothermal therapies). Our method has high spatial and spectral resolution, high sensitivity, and can also provide real time information, which are important features for *in vivo* applications.

In order to implement molecular imaging with this approach, this work must be extended to include the bioconjugation of these nanoparticles to active-targeting antibodies, which can target molecules such as cell receptors. The utilization of their distinct absorption spectra makes it possible to achieve multiplexed molecular detection *in vivo* [17].

Acknowledgments

The authors acknowledge Hillel Price and Sanghoon Kim for their assistance in the preparation of silvered coverslips, and Jun Wang for her help in cell culture. This work is funded by grants from the National Institutes of Health (NCI 1 R01 CA138594-01).

#170037 - $15.00 USD Received 7 Jun 2012; revised 18 Jul 2012; accepted 18 Jul 2012; published 20 Jul 2012